TU Delft

Delft University of Technology

Analysis of embankment underlain by elastic half-space
2.5D model with paralongitudinal approximations to the half-space

Kausel, Eduardo; Barbosa, João Manuel de Oliveira

DOI
10.1016/j.soildyn.2021.107090

Publication date
2022

Document Version
Final published version

Published in
Soil Dynamics and Earthquake Engineering

Citation (APA)
Kausel, E., & Barbosa, J. M. D. O. (2022). Analysis of embankment underlain by elastic half-space: 2.5D model with paralongitudinal approximations to the half-space. *Soil Dynamics and Earthquake Engineering*, *155*, Article 107090. https://doi.org/10.1016/j.soildyn.2021.107090

Important note
To cite this publication, please use the final published version (if applicable).
Please check the document version above.

Copyright
Other than for strictly personal use, it is not permitted to download, forward or distribute the text or part of it, without the consent of the author(s) and/or copyright holder(s), unless the work is under an open content license such as Creative Commons.

Takedown policy
Please contact us and provide details if you believe this document breaches copyrights.
We will remove access to the work immediately and investigate your claim.

This work is downloaded from Delft University of Technology.
For technical reasons the number of authors shown on this cover page is limited to a maximum of 10.

Green Open Access added to TU Delft Institutional Repository

'You share, we take care!' - Taverne project

https://www.openaccess.nl/en/you-share-we-take-care

Otherwise as indicated in the copyright section: the publisher is the copyright holder of this work and the author uses the Dutch legislation to make this work public.

Soil Dynamics and Earthquake Engineering 155 (2022) 107090

Contents lists available at ScienceDirect

Soil Dynamics and Earthquake Engineering

journal homepage: www.elsevier.com/locate/soildyn

Analysis of embankment underlain by elastic half-space: 2.5D model with paralongitudinal approximations to the half-space

Eduardo Kausel [a,*], João Manuel de Oliveira Barbosa [b]

[a] Massachusetts Institute of Technology, Cambridge, MA, 02139, USA
[b] Technical University, Delft, Netherlands

ARTICLE INFO

Keywords:
Dispersion spectra
Waves in layered media
Moving loads
Critical speed
Fast rail

ABSTRACT

This article presents a set of close approximations to model an elastic half-space supporting an embankment, which are evaluated in the context of phase velocity spectra, i.e. in terms of the normal wave propagation modes of the embankment-half-space system. The ultimate, intended target of these approximations is in the modeling of vertically-acting loads that may travel over the embankment with some prescribed, constant longitudinal speed. The proposed approximations are analogous to the well-known paraxial approximations that closely mimic a half-space terminating at a plane boundary, but differ from these in that the approximations herein aim at properly modeling not the waves with near normal incidence to the half-space, but waves which propagate at shallow, grazing angles along the longitudinal direction of load motion. Thus, these can be referred to as *paralongitudinal* approximations. The resulting expressions allow for a very effective simulation of the system at hand for loads moving with subcritical speed and solved in the context of a 2.5D solution method. Such 2.5D formulation considers a continuous model in the longitudinal direction and a discrete model in transverse planes.

1. Introduction

One of the most effective numerical tools available for the analysis of loads moving over an embankment relies on a semi-discrete formulation of the equations of motion cast in the 2.5 dimensional space. It is based on employing analytical tools for the solution in the direction of the embankment —which is also the direction of motion of the load— and a discretization with finite elements in the two transverse directions. This method is closely related to the widely known *Thin Layer Method* (TLM), which discretizes the space in just one direction, namely the depth [1–4]. Unlike the TLM, which presupposes horizontal layering, in this alternative the material properties are allowed to change in the plane of the discretized cross-section, in which case the embankment can roughly be visualized as a bundle of spaghetti in which each of the threads is allowed to be materially different from the neighboring ones, even if each is unchanging in the longitudinal direction. Each thread has then a cross-section in the shape of the underlying finite elements used and —at least initially— is infinitely long in the longitudinal direction. For this reason, and in analogy to the TLM, this formulation is probably best referred to as the *Thin Tube Method* (TTM). In chapter 3 of his PhD dissertation [5], Barbosa describes this method in detail while referring to it as the *2.5D Finite Element Method* (2.5D-FEM). A slew of other researchers have also made use of the 2.5D method in Refs. [6–13]. A sketch for this approach is shown in Fig. 1.

It is clear, however, that most embankments are not supported by rigid ground, but are underlain instead by deformable ground that to a good approximation could be modeled as a homogeneous elastic half-space. This half-space not only introduces an additional waveguide along which waves may propagate, but allows waves to enter the half-space and dissipate there in the form of *radiation damping*. The problem with that is that the addition of the spatially unbounded half-space introduces significant technical difficulties in the 2.5D approach. Although ultimately these can be overcome by an adequately sophisticated model for the half-space, that extracts in turn a steep price: the numerical solution requires far more effort and is also prone to numerical errors which arise when interfacing and coordinating the various parts of this problem.

For example, one alternative is to use a Green's functions formalism for the half-space and assess the flexibility at the discrete nodes along the interface with the embankment in terms of the longitudinal wavenumber. The problem with that is not only that the calculation and subsequent inversion of the flexibility matrix into a dynamic stiffness

* Corresponding author.
E-mail address: kausel@mit.edu (E. Kausel).

https://doi.org/10.1016/j.soildyn.2021.107090
Received 25 July 2021; Received in revised form 18 November 2021; Accepted 22 November 2021
Available online 7 February 2022
0267-7261/© 2021 Elsevier Ltd. All rights reserved.

matrix is computationally intensive —an integral must be solved in the transverse wavenumbers— but also that the variation of that stiffness matrix depends in a complicated way on the axial wavenumber and frequency. This is because both the horizontal wavenumber and the frequency remain "hidden" inside square root terms, and these prevent a direct representation in terms of constant stiffness and mass matrices, as is the case with the embankment itself. In this article, we express the half-space in terms of simple yet provably accurate mechanical devices that have stiffness and mass properties similar to those of the embankment, and therefore, allow a more direct solution for problems of this kind.

2. Classical approach to dynamic loads acting with a layered medium

Consider a horizontally layered medium that is subjected to a dynamic source at some location, say at the free surface. When the equations of motion to that problem are formulated in either two or three dimensions, it is found that the exact solution is ultimately cast in terms of Fourier and/or Hankel transforms that involve improper integrals over frequencies ω and over either horizontal or radial wavenumbers k, as detailed in Refs. [14,15]. Although these integrals can be solved numerically, that alternative is fraught with perils and difficulties because of three main reasons:

1. The integrals must be truncated at some upper limit, yet the integrands may decay only slowly with wavenumber;
2. For lightly-damped (or even undamped) media the integrands contain a finite number of near singularities that must be dealt with appropriately; these occur at the near resonances of the system, or at the true resonances for media of finite depth (an *open*, unbounded system has no true resonant frequencies, but reflections at material discontinuities can lead to standing wave patterns occurring at some frequencies for which the response is large, even if not infinitely so); and
3. The integrals must be replaced by discrete summations, which require choosing an adequately small step in frequencies and wavenumbers. But at the very moment that those integrals are discretized, that introduces *eo ipso* a periodicity in both space and time. This occurs because of the so-called *aliasing* problem of signal processing. At least partially, that aliasing problem can be overcome by using complex frequencies in the context of a numerical formulation of the inverse Laplace transform in terms of a Fourier transform [16].

The most common way to overcome the difficulties alluded to above is to carry out contour integrations in the complex plane and express the displacements at any arbitrary point in terms of the normal modes of wave propagation. For each given frequency ω, the normal modes method seeks the horizontal or radial wavenumbers $k_j, j = 1, 2, \cdots$ that satisfy the eigenvalue problem associated with the homogeneous elastic equations, i.e., the free vibration solutions that may be found in the absence of sources. Or alternatively, given the longitudinal wavenumber k, one seeks the frequencies ω_j that satisfy that same eigenvalue problem. Once these modes have been determined, the solution for displacements at arbitrary points is then expressed in terms of a modal superposition.

In the case of stratified media of *finite depth* (i.e., plates or strata) it is found that at any fixed frequency ω there exist only a finite number of wave propagation modes with real wavenumber k_j, and an infinite number of such modes with complex wavenumbers. The former constitute the classical wave propagation modes or proper *normal modes* that can still be detected at remote distances from a dynamic source, while the latter constitute the evanescent modes, which can be detected only in the immediate vicinity of sources. It can also be shown that the exact, complete solution can be expressed by superposition of *all* of these modes, real and complex, that is, that the *modal set is complete*. In those cases, and for practical purposes, it suffices to consider the finite number of real modes together with a small, finite subset of those evanescent modes whose characteristic wavenumber has a suitably small imaginary part. Although the modes themselves can be found by means of the so-called search techniques, a far more convenient and direct approach is to make use of the Thin-Layer Method. That way, the eigenvalue problem reduces to either a linear or a quadratic eigenvalue problem for which standard methods in linear algebra can be used [1].

On the other hand, in the case of undamped, layered media underlain

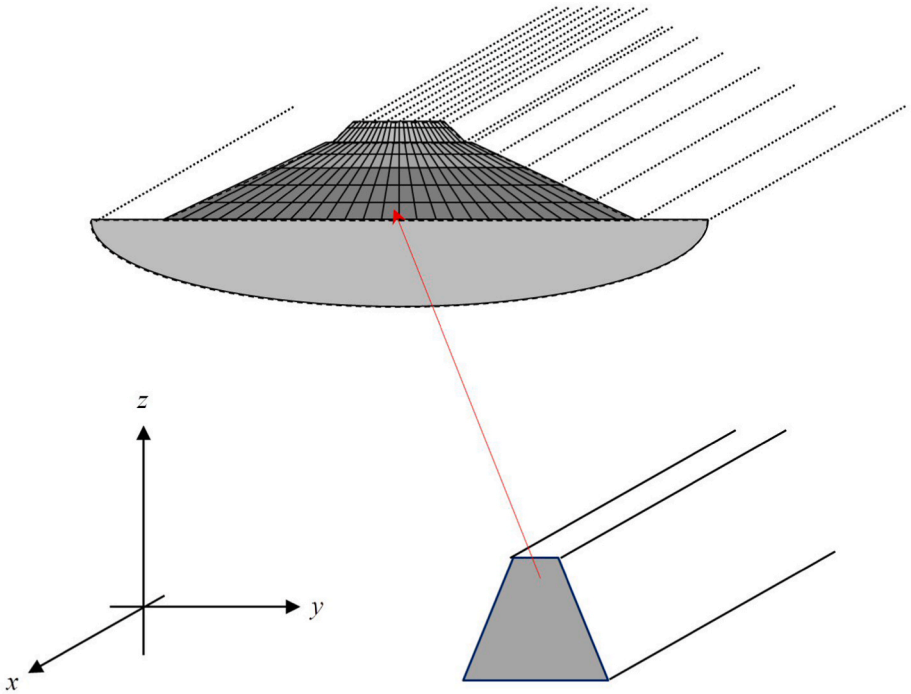

Fig. 1. Embankment composed of 2.5D elements.

by infinitely deep half-spaces, there exist only a finite number of real modes, and no complex modes whatsoever —or at least none that are physically realizable. This can be demonstrated quite easily: if there existed a complex mode, say $\overline{k}$, then the two dispersion conditions for the half-space, which relate horizontal and vertical wavenumbers for both P and S waves, would be of the form

$$\overline{k}^2 + k_{zP}^2 = (\omega/\alpha)^2 \ , \ \overline{k}^2 + k_{zS}^2 = (\omega/\beta)^2 \tag{1}$$

where α, β are the P and S wave velocities in the half-space.

But if $\overline{k} = a - \mathrm{i}b$, $a, b > 0$ such that $\exp[\mathrm{i}(\omega t - ax)]\exp(-bx)$ is a wave that propagates left to right and also decays in that direction (i.e., an evanescent wave), then that would imply

$$k_{zP} = \pm\sqrt{(\omega/\alpha)^2 - a^2 + b^2 + 2\mathrm{i}ab} \tag{2}$$

which is a complex number that lies in either the first or third quadrant, i.e., $k_{zP} = \pm(c + \mathrm{i}\, d)$, $c, d > 0$ which, in turn, would imply a variation in the vertical direction $\exp[\mathrm{i}(\omega t - cz)]\exp(dz)$. Such a wave propagates upwards and decays downwards, in which case it fails to satisfy the *radiation condition* at $z = -\infty$, because wave energy originates at an infinite depth. Or alternatively, it propagates down and grows in that direction without any bound, in which case it fails the *boundedness condition*. Either way, we conclude that no complex, evanescent waves can exist.[1]

Both the finite number of real modes as well as the lack of complex modes already indicates that the modal superposition is in itself not complete when the system includes a half-space. For example, the homogeneous half-space has only one mode, namely the Rayleigh wave, which is certainly not sufficient to describe motions at arbitrary locations. As it turns out, the contour integration then produces another set of non-singular, improper integrals referred to as branch integrals, the details for which need not concern us here. These do take care of the missing mix of body waves, some of which radiate into the half-space and give rise to "radiation damping".

2.1. Dispersion spectra

Consider a medium of either finite or infinite depth, which may or not exhibit horizontal layering. Let also $\mathbf{x} = (x, y)$ define the horizontal coordinates and z the depth coordinate (either up or down, as may be preferred). This system may in turn be subjected to dynamic sources or body loads $\mathbf{b}(\mathbf{x}, t)$ than can act anywhere. In small strain elasticity, such problem is characterized by a set of second order, partial differential equations in the displacements $\mathbf{u} = \mathbf{u}(\mathbf{x}, z, t)$ of the form

$$\mathrm{L}(\mathbf{u}) = \mathbf{b} \tag{3a}$$

$$\mathrm{B}_i(\mathbf{u}) = \mathbf{0} \ , \ i = 1, 2, \cdots n \tag{3b}$$

where L , B_i are appropriate linear, partial differential operators in x, y, z, t, and n = number of boundary conditions at each boundary point.

Now, if the sources are absent at all times $\mathrm{L}(\mathbf{u}) = \mathbf{0}$, then the set equations is said to be *homogeneous*. Such equations admit non-trivial solutions within a class of free waves which can exist and propagate on their own. An example of these is the Rayleigh mode observed at the surface of an elastic, homogeneous half-space.

Assuming that the system is free from sources, then after carrying out a triple Fourier transform in the horizontal space coordinates and in time, we are led to a homogeneous system of ordinary differential equations in z in which the unknown field is of the form

$$\mathrm{L}_z(\widetilde{\mathbf{u}}) = \mathbf{0} \ , \ \mathrm{B}_i(\widetilde{\mathbf{u}}) = \mathbf{0} \tag{4a}$$

$$\widetilde{\mathbf{u}} = \widetilde{\mathbf{u}}(\mathbf{k}, \omega, z) \ , \mathbf{k} = \left(k_x, k_y\right) \ = \ \text{horizontal wavenumbers;} \ \omega = \text{frequency} \tag{4b}$$

If we take ω as a parameter and fix it at some known value, then the wave propagation problem becomes an eigenvalue problem in the horizontal wavenumbers. For a horizontally stratified medium that is isotropic in the plane, the eigenvalue problem above reduces to that of plane (i.e. 2-D) waves with effective horizontal wavenumber $k = \sqrt{k_x^2 + k_y^2}$ which propagate along the arbitrary direction $\vartheta = \arctan(k_y / k_x)$. In that case, we are led to the simpler 2-D eigenvalue problem for $\widetilde{\mathbf{u}} = \widetilde{\mathbf{u}}(k, \omega, z)$, the details of which are well known and need not be repeated herein. The solutions to the eigenvalue problems are then of one of the two forms

$$\widetilde{\mathbf{u}} \to \boldsymbol{\psi}_n \exp \mathrm{i}[(\omega\, t - k_n x)] \ , \quad k_n = k_n(\omega) \quad \omega \text{ is a fixed real parameter} \tag{5a}$$

$$\widetilde{\mathbf{u}} \to \boldsymbol{\varphi}_n \exp \mathrm{i}[(\omega_n\, t - k\, x)], \quad \omega_n = \omega_n(k) \quad k \text{ is a fixed real parameter} \tag{5b}$$

in which $n = 1, 2, \cdots$ is the modal index and $\boldsymbol{\varphi}_n(z), \boldsymbol{\psi}_n(z)$ are the corresponding eigenvectors.

In either option, we also define

$$V_{ph} = \frac{\omega}{k} \quad = \text{ phase velocity} \tag{6a}$$

$$V_g = \frac{d\omega}{dk} \quad = \text{ group velocity} \tag{6b}$$

where $k = k_n$ in the first option, or $\omega = \omega_n$ in the second and whenever these are real quantities. That is, the phase and group velocities have multiple, distinct branches $V_{ph} = V_{ph}(f)$, $V_g = V_g(f)$, $f = \frac{1}{2\pi}\omega$ which collectively form the so-called *dispersion spectra*, as will be illustrated later on.

When choosing the horizontal wavenumber as a real parameter, and in the absence of damping, the eigenvalues ω_n can be shown to be always real and non-negative, as can be demonstrated rigorously. Thus, in that case all phase velocities are real as well.

2.2. 2-D half-space approximations

As shown in Ref. [14] and improved upon in Ref. [15], the *exact* 2-D in-plane (SV–P) and anti-plane (SH) impedances (or dynamic stiffnesses) of the half-space in the frequency-wavenumber domain and per unit area are

$$\mathbf{K}_{SVP} = 2k\mu\left[\frac{1 - s^2}{2(1 - ps)}\begin{Bmatrix} p & -1 \\ -1 & s \end{Bmatrix} + \begin{Bmatrix} 0 & 1 \\ 1 & 0 \end{Bmatrix}\right], \quad K_{SH} = ks\mu \tag{7}$$

where μ is the shear modulus of the half-space, and the terms in p, s (which are proxies for the vertical wavenumbers for P and S waves $k_{Pz} = \mp\mathrm{i}\, kp$, $k_{Sz} = \mp\mathrm{i}\, ks$) are defined as

$$p = \sqrt{1 - \left(\frac{\omega}{k\alpha}\right)^2}, \quad s = \sqrt{1 - \left(\frac{\omega}{k\beta}\right)^2} \tag{8}$$

with α, β being the P and S wave velocities in the half-space. As can be seen, both the frequency and the wavenumber are contained within a square root term. This implies in turn that when these impedances are added at the bottom of a discrete formulation for the layers in the context of the TLM, the resulting equations contain terms in k, ω that

[1] In a strictly mathematical sense, one can certainly find complex solutions for *non-physical modes* which fail the radiation or boundedness conditions, or both; some authors refer to these as the "forbidden modes", or as the modes in the lower Riemann sheet. These can be useful in the solution of certain problems in which displacements within a finite, bounded region are expanded in terms of basis function composed of nonphysical modes, just as well as mathematical functions can be expanded in terms of Maclaurin series that converge only within a circle of given radius around the expansion point, even if they fail to converge elsewhere.

remain "hidden" or "implied". This then leads to transcendental eigenvalue problems that are not amenable to simple solutions.

There exist two alternatives to circumvent this problem. The first, which was proposed by Kumar & Naskar [17], consists in choosing the phase velocity $V_{ph} = \omega/k$ instead of the horizontal wavenumber k as a free parameter. Then

$$p = \sqrt{1 - \left(\frac{V_{ph}}{\alpha}\right)^2}, \quad s = \sqrt{1 - \left(\frac{V_{ph}}{\beta}\right)^2} \tag{9}$$

which are both real quantities whenever $V_{ph} \le \beta$. That implies in turn that the variation of displacements in the half-space decays exponentially with depth. By contrast, if $V_{ph} > \beta$, then either s or both s, p become complex, and with that, the eigenvalue ω_n becomes complex. If so, the wave radiates energy into the half-space while violating the boundedness condition at an infinite depth. Thus, this must be rejected.

The second alternative consists in finding polynomial approximations to p, s for small values of the phase velocity by means of Taylor series with $V_{ph}/\beta < 1$, which is what we shall explore in the ensuing. We start by writing the SVP half-space impedance as

$$\begin{aligned} &\mathbf{K}_{SVP} = \mu k \begin{Bmatrix} z_{11} & z_{12} \\ z_{12} & z_{22} \end{Bmatrix} = \mu k\, \mathbf{Z} \\ &A = \frac{1 - s^2}{1 - ps}, \xi = \frac{\omega}{k\beta}, a = \frac{\beta}{\alpha}, s = \sqrt{1 - \xi^2}, p = \sqrt{1 - a^2\xi^2} \\ &z_{11} = Ap, z_{12} = 2 - A, z_{22} = As \end{aligned} \tag{10}$$

To avoid mistakes, we proceed next to make use of the Matlab script given in Appendix 1. When this is carried out, we ultimately find

which is quadratic in the frequency for any given (fixed) wavenumber k, where $\omega/(k\beta) = V_{ph}/\beta$. These are then the approximate impedances for

$$\mathbf{K}_{SVP} \approx k\mu\mathbf{Z} = k\mu \left\{ \frac{2}{1 + a^2} \begin{bmatrix} 1 & a^2 \\ a^2 & 1 \end{bmatrix} - \left(\frac{\omega}{\beta k}\right)^2 \frac{1}{2(1 + a^2)^2} \begin{bmatrix} 1 + 3a^4 & -(1 - a^2)^2 \\ -(1 - a^2)^2 & 3 + a^4 \end{bmatrix} \right\} \tag{11}$$

SVP waves in the half-space.

The SH case is much simpler and we find

$$K_{SH} = ks\mu \approx k\mu \left[1 - \frac{1}{2}\left(\frac{\omega}{k\beta}\right)^2\right] \equiv k\mu \left[1 - \frac{1}{2}\left(\frac{V_{ph}}{\beta}\right)^2\right] \tag{12}$$

An interesting and revealing question is now: What kind of waves does this approximation imply when the half-space is *not* overlain with any layers? That is, what kind of "Rayleigh waves" would it imply? This corresponds to the condition $|\mathbf{K}| = 0$ i.e. $|\mathbf{Z}| = 0$. Using Matlab, the roots are ultimately found to be

$$\xi^2 = \frac{\pm\sqrt{2}}{\sqrt{1 + a^4}} \sqrt{2 - a^2(1 - a^2) \pm \sqrt{3a^8 - 2a^6 + 5a^4 - 4a^2 + 2}}\,, a \le \frac{1}{2}\sqrt{2},\ \xi = V_{ph} \Big/ \beta \tag{13}$$

Fig. 2 shows the smallest positive root $\xi = \xi(\nu)$ as function of Poisson's ratio ν in the interval $0 \le \nu \le 0.5$, after substituting $a = \beta/\alpha = \sqrt{(1 - 2\nu)/(2 - 2\nu)}$. That root for ξ exceeds slightly the speed of shear waves, and with that, also slightly the speed of Rayleigh waves in the half-space which, depending on Poisson's ratio, ought to lie in the interval $[0.874 \le V_R/\beta \le 0.955]$. But the error is no larger than about 10%. Therefore, we are confident that the half-space approximation will work well when finding the *real* eigenvalues for a layered medium, as considered in the next example.

2.2.1. Example: Layered medium over elastic half-space, exact vs. approximate solutions

Consider a system of layers underlain by an elastic half-space with the material properties listed in Table 1. Observe that the last layer in this profile has the same properties as the half-space underneath, so it would normally be disposed of whenever the half-space representation is exact. Here, this *buffer layer* is retained deliberately so as to improve the performance of the half-space approximations, see also Appendix 2 for further details.

When this problem is solved using first the exact impedances for the half-space, and thereafter using the approximate impedances, we find the dispersion spectrum shown in Fig. 3. The two solutions are depicted in blue and red, respectively, and for the most part perfectly overlap with one another (color in online version only). Indeed, the agreement is nearly perfect throughout, except for a tiny loop at $V_{ph} = 150$ m/s, $f = 50$ Hz that is missing in the approximate solution and some quite acceptable deviations in the first branch at very low frequencies, at which the true branch starts at the Rayleigh wave speed of the half-space while the approximate does so at the shear wave speed. Other examples with alternative soil profiles yielded equally good results —as does the SH case too— so they need not be shown. We conclude then that the half-space approximations proposed are very good indeed.

A word in closing: An informed reader may perhaps have wondered what, if any, connections do these approximations have with the well-known paraxial approximations for a half-space. The short answer is that they are very different. Indeed, the word "*paraxial approximations*" indicates that these are intended to model waves that propagate close ("para") to the normal to the boundary (the "axis"). In the case of a half-space with a horizontal boundary, those would be waves that propagate nearly vertically, i.e. are *paravertical*. Those waves have small horizontal wavenumbers k and propagate at a small angle to the vertical $\theta = \arcsin(k/k_s)$, $k < k_s$, $k_s = \omega/\beta$. Here, by contrast, we are seeking approximations for shallow waves in the half-space that propagate nearly horizontally, that is, are *paralongitudinal*. Such waves do not propagate down but decay exponentially with depth, or at least this is so in the half-space. In other words, now the horizontal wavenumber exceeds the shear wave number $k > k_s$. This is also the reason why we take Taylor series with respect to small values of $k_s = \omega/\beta \to 0$.

Then again, when applying the proposed approximations in the context of moving loads that move with velocity below the critical speed at which the response grows without any bound [18], it will be found that there are no waves that propagate either down into the half-space or laterally along the surface, and this is the reason for why the proposed method is applicable in that case. Indeed, if such waves existed, they would radiate energy away from the moving load and damp out the

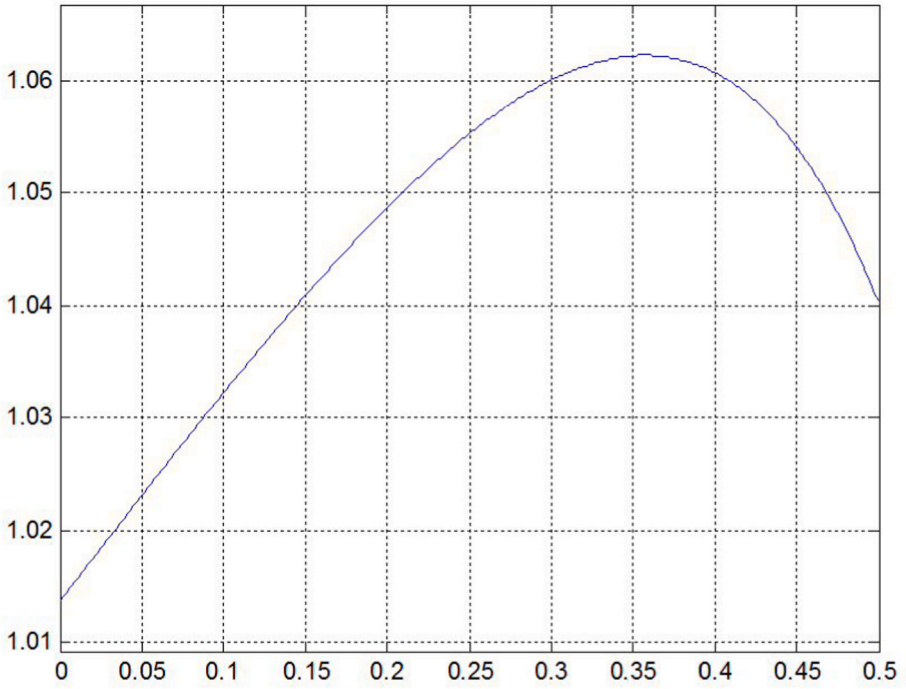

Fig. 2. Approximate eigenvalue for a homogeneous half-space vs Poisson's ratio.

solution. Still, such waves may well exist in the super-critical regime $V > V_{cr}$ (where V is the speed of the load and V_{cr} is the critical speed), in which case the only way to have a steady-state (Galilean-type) solution would be for the load to recline back a little. That would add a small horizontal component F_x supplying the power $\Pi = F_x V$ needed to compensate for the energy lost to radiation. But in that regime, the approximations given herein would cease to work as intended.

2.3. Applications to 2.5D embankments

Consider an embankment for a high-speed rail line that is underlain by a homogenous, elastic half-space. When the TTM is used to discretize the embankment, we are led to a discrete element mesh in the plane $y-z$ that is continuous in the axial direction x, as shown in Fig. 1. The nodes of this mesh along the bottom interface are in contact with the elastic half-space, to which they are bound. The elastic response of the half-space is then captured by means of the discrete approximation presented earlier. For this purpose, we proceed to lump at each of the inner node an impedance matrix

$$\mathbf{K}_{approx} = \ell \begin{bmatrix} K_{xx}^{SVP} & 0 & K_{xz}^{SVP} \\ 0 & K_{yy}^{SH} & 0 \\ K_{zx}^{SVP} & 0 & K_{xx}^{SVP} \end{bmatrix} \tag{14}$$

where ℓ is the inter-nodal distance, which we assume to be uniform, and the elements of this matrix follow from the preceding. For the outer nodes at the intersection of the slopes of the embankment with the half-space, we use half as much, since those nodes receive contribution from one side only. We mention in passing that this simple way of adding approximate impedances to the discrete nodes along the embankment-half-space interface contains one additional approximation. Indeed, it distributes *plane-strain* stiffnesses for longitudinal waves and neglects wave propagation in the lateral direction. In short, the approximations are functions of the longitudinal wavenumber only. This should not have a major effect while greatly simplifying the half-space model.

One last observation: In an actual implementation it is necessary to consider also an implied imaginary factor in one or two of the components, which is done to achieve symmetric matrices. In addition, the off-diagonal signs must be reversed if the vertical axis points down, not to mention changing appropriately the locations of the matrix elements whenever the coordinate axes are taken in some other order, say with the y axis being the longitudinal one. These are, however, details that are rather familiar to those who make regular use of the TLM and TTM methods, and are described in detail in Ref. [5], in which case they need not be elaborated upon herein.

2.4. Dispersion spectra for an embankment

Consider an embankment with the simple cross-section shown in Fig. 4, in which only the right half of the mesh is used on account of symmetry. The embankment rests on a homogeneous half-space, of which an upper buffer layer of the same properties as the half-space is added so as to improve the accuracy of the solution. The springs at the bottom of the buffer region correspond to the half-space stiffness approximations given by the matrix $\mathbf{K}_{approx}$. The refinement of the mesh is dictated by the highest frequency of interest, i.e. the shortest possible wavelength, which is estimated as $\lambda_{\min} = \beta_{\min}/f_{\max}$. The standard recommendation is 6 elements per wavelength for linear elements, and 3 elements per wavelength for quadratic elements. But considering the fact that in a 2.5 D model most of the waves will be propagating in the longitudinal, continuous direction, and less so consist of lateral reverberations, this criterion could be relaxed somewhat, especially because the element size is conservatively being defined at the highest frequency, and not at the typical or dominant frequency of the response.

Table 1
Soil profile.

Layer	β [m/s] Shear wave velocity	ρ [Mg/m^3] Mass density	ν Possion's ratio	h [m] Thickness
1	250	1.6	0.25	0.35
2	300	2.3	0.30	0.30
3	250	2.2	0.30	0.50
4	100	2.0	0.30	1.50
5	150	2.0	0.30	3.00
6	150	2.0	0.30	∞

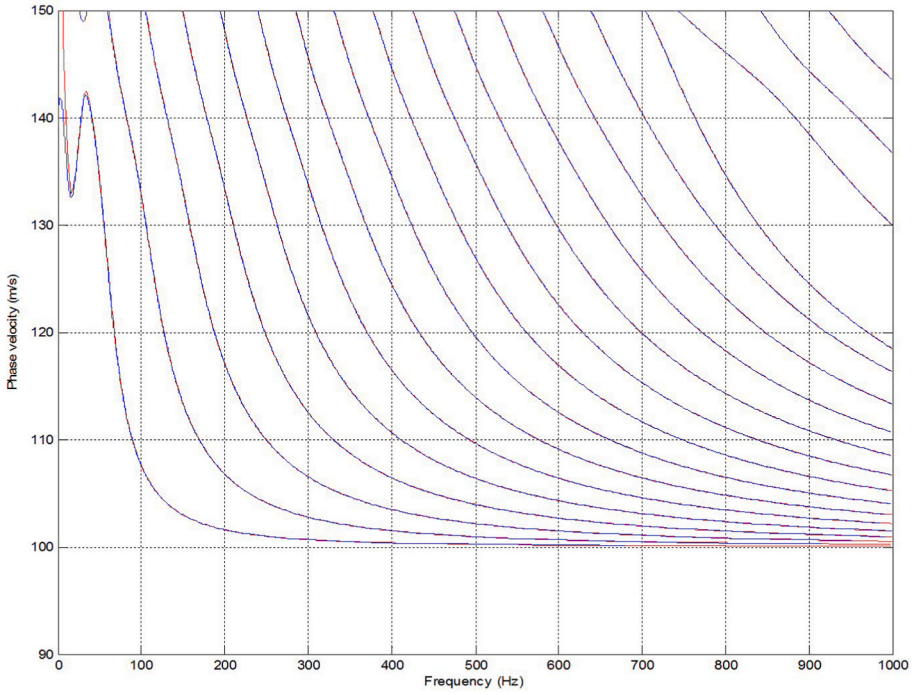

Fig. 3. Dispersion spectrum, comparison of exact (blue) vs. approximate (red). [Note: Color in online version only]. (For interpretation of the references to color in this figure legend, the reader is referred to the Web version of this article.)

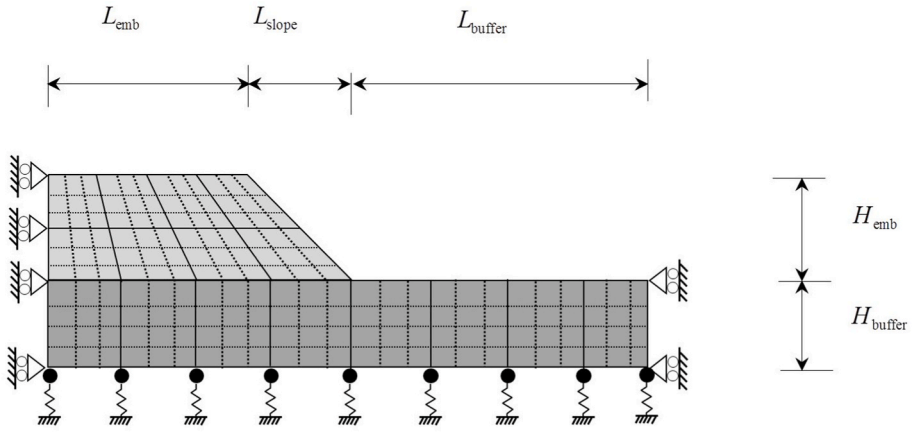

Fig. 4. Discrete 2.5D model (schematic only).

Taking advantage of the geometric symmetry, the discrete model can be reduced in size such that only half of the embankment is needed. This is accomplished by cutting out the right half and adding appropriate boundary conditions at the left edge of the model that represents the mid-plane. As shown schematically in Fig. 4, for symmetric modes the boundary conditions required are vertical rollers, while the anti-symmetric modes would require horizontal rollers. But inasmuch as the antisymmetric modes play no role when the vertical traveling load is applied at the upper surface in the mid-plane, this second set of boundary conditions will not be considered herein.

With reference to the material properties listed in Table 2, the depth of the embankment is chosen to be that of layer 1, namely $H_{\text{emb}} = 0.6$ m, and its half-width at the top is $L_{\text{emb}} = 2.5$ m. Choosing also the lateral slopes to have an inclination of 45°, then the added half-width is $L_{\text{slope}} = 0.6$ m so that the total half-width at the bottom is 2.5+ 0.6 = 3.1 m. A buffer layer of total depth $H_{\text{buffer}} = 5$ m with the same material properties of the half-space is added at the bottom for increased accuracy (see also Appendix 2). Here we arbitrarily choose the total width of the buffer layer to be equal to the width of the embankment, i.e. $L_{buffer} = 0$. The cross-section is then discretized into quadrilateral elements of maximum dimension 0.1 m, which results in a mesh of the type shown schematically in Fig. 4 but much more refined and deeper than shown —this is to allow for proper labeling of the figure.

We comment in passing that Fig. 4 does not show any loads being applied onto the discrete model because only the spectral lines for phase

Table 2
Soil profile of embankment and half-space for 2.5-D example.

Layer	β [m/s] Shear wave velocity	ρ [Mg/m^3] Mass density	ν Possion's ratio	h [m] Thickness
1	200	1.6	0.20	0.60
2	300	2.0	0.35	∞

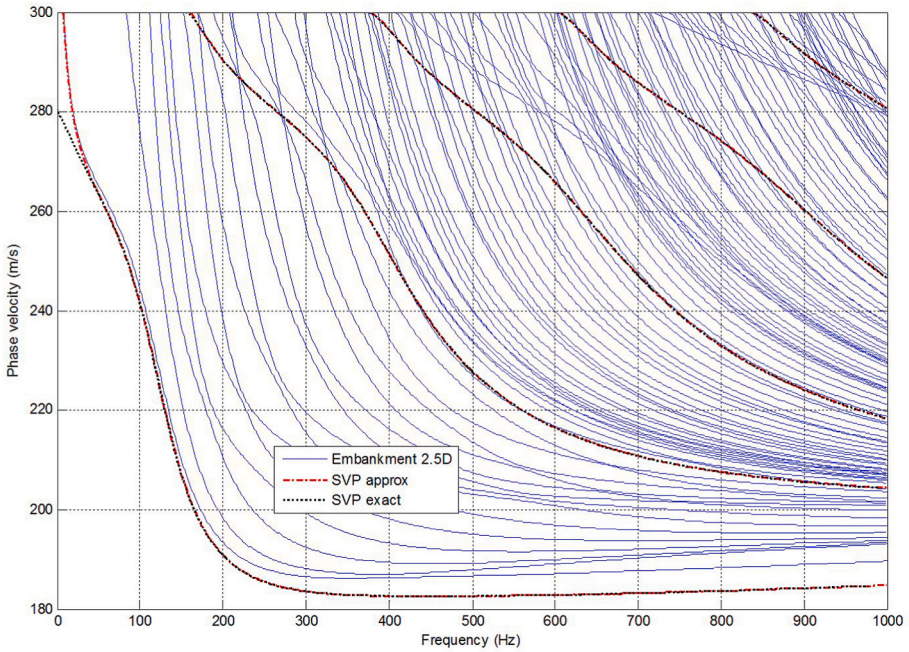

Fig. 5. Phase spectra for embankment underlain by an elastic half-space. Solid blue lines = 2.5D embankment model; dashed red lines = approximate 2D phase velocity spectra for SVP waves; black dotted lines = exact 2-D spectrum. [Note: Color in online version only]. (For interpretation of the references to color in this figure legend, the reader is referred to the Web version of this article.)

velocities are being considered herein.

Fig. 5 shows the spectral lines of the *symmetric* modes for the problem at hand while restricting the number of 2.5D modes so as to save in computation time. To help in the interpretation of the spectra obtained, we have also added in black and red dashes the 2-D modes for SVP waves in a layered half-space with the same material properties as in Table 2. We computed these spectral curves with both the *exact* formulation (black dotted curves) and the approximate half-space impedances (red dashed curves). The antisymmetric modes could readily be obtained with the same formulation while using alternative boundary conditions for the model.

Within the frequency range shown, there are four such SVP modes. Of these, the fundamental SVP mode shown in red practically coincides with the fundamental embankment mode, merely showing a modest discrepancy in the very low frequency range below some 25 Hz or so; this is certainly an artifact caused by the half-space approximation added at the bottom of the 2.5 D model, as can be seen by comparing the first red (approximate) and first black (exact) curves for the plane strain

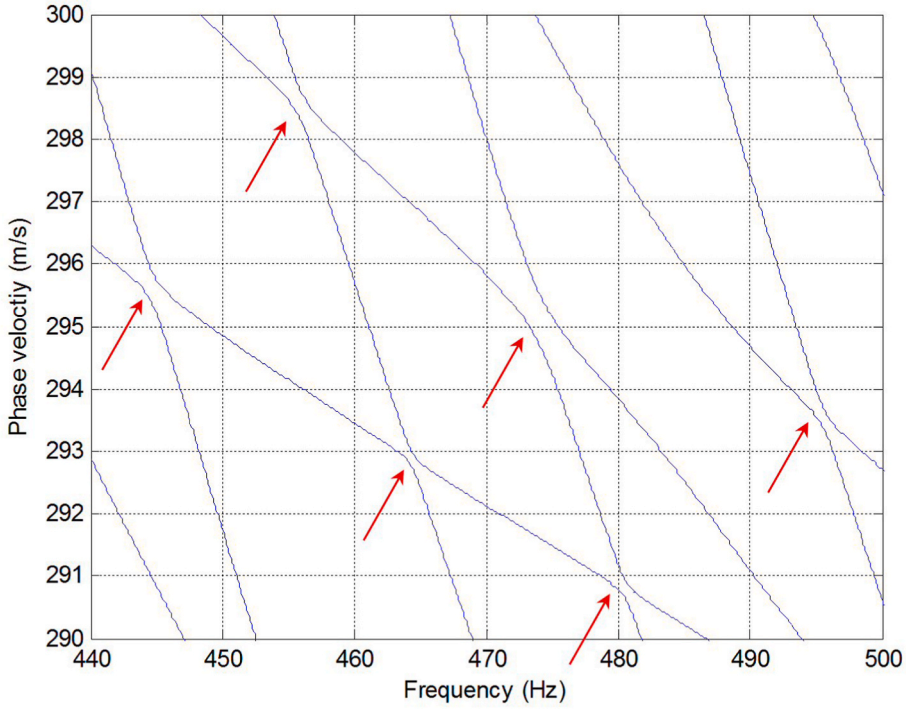

Fig. 6. Amplified spectrum showing the osculation points.

spectra. The true spectral curve for the fundamental mode starts at the Rayleigh wave speed of the half-space, while the approximate one starts at the shear wave velocity of that half-space. This occurs because the typical wavelengths at very low frequencies exceed the depth of the discrete model. Indeed, at a phase velocity of $V_{ph} = 150$ m/s and frequencies well below $f = 25$ Hz, the wavelengths will be longer than $\lambda > 150/25 = 6$ m, which already exceeds the total depth of the discrete model used. If the physical problem being studied were to involve mainly low frequencies, then a simple remedy to the spectral artifact could consist in using a coarser finite element mesh with a thicker buffer layer, say increase from 5 m to perhaps 10 or 15 m. That coarser and deeper model will surely improve matters considerably —at least in the low frequency range, if that were all that is needed. As for the other two higher modes, their error is much less and they too merge with modes of the embankment. Finally, and at least in principle, one could refine the mesh as the frequency increases, but that is surely not very practical, and it could lead to other artifacts related to the fact that the more refined meshes have more degrees of freedom and thus more modes. That would also greatly complicate modal superposition.

It is patently clear that the embankment displays a combination of the plane strain SVP modes plus a slew of other modes that ultimately are non-planar SVP modes propagating at some angle with respect to the longitudinal axis and reverberating laterally back and forth between the slopes as they advance in the longitudinal direction. In the case of the antisymmetric modes (not shown, but which could be excited by non-symmetric sources) such additional modes will include also helical modes (torsional modes).

In addition to the laterally reverberating modes, there exist also a number of modes that still propagate mainly in the longitudinal direction yet remain locally confined to the sloping part. These are similar to the SVP modes for a shallower depth of soil over elastic half-space, which causes their phase speeds to be higher when compared with those which dominate near the center of the embankment. These are modes whose modal amplitudes are significant only within the slopes, and are especially noticeable when softer layers outcrop on the slopes and become exposed there.

The phase velocity spectrum in Fig. 5 also exhibits many points at which the branches seem to cross each other. Upon magnification it is seen that these are merely apparent crossings, as demonstrated in Fig. 6. It is seen that these apparent crossings constitute osculation points at which branches come exquisitely close together, only to avoid contact with each other in their very closest approach [19]. Still, amongst the waves that reverberate laterally in a geometric and materially symmetric embankment of finite width, the spectral branches of the uncoupled symmetric and antisymmetric modes will surely exhibit plenty of crossings with each other even if not with themselves. This concept helps significantly when sorting out spectral branches obtained numerically.

2.5. Application to moving loads such as in high-speed rail

It is well-known that the response of an embankment caused by moving loads can be formulated and obtained in the frequency domain in terms of the normal modes of wave propagation of the system. That is, the response functions are obtained by modal superposition. Hence, if the dispersion spectra for waves in the embankment-half-space system are provably accurate, then so will also be the response functions. Thus, there is no doubt in our minds that the proposed model will be accurate when used in the context of moving loads.

However, we emphasize that the approximate impedances for the half-space used are predicated on the assumption that the travel velocity of the load does not exceed the speed of shear waves in the half-space, i.e. they are not *transonic*, because that was one of the key assumptions in the development of the half-space approximations. Inasmuch as the system behavior changes dramatically once this physical barrier is crossed, i.e. once the load becomes *supercritical* [18], the approximations will break down and be useless in the domain of very high speeds.

In the preceding we focused solely on the dispersion spectra for the symmetric modes, i.e. those that exhibit symmetry with respect to the vertical mid-plane. In fact, these are the only modes that will be excited by moving loads that in the transverse direction are symmetrically distributed, such as a single rail line at the center of the embankment. If the loads were non-symmetric, say an embankment with two rail lines, that load would in addition require the determination of the wave spectra for antisymmetric loads, inasmuch as non-symmetric loads can always be expressed as a superposition of symmetric and antisymmetric loads. Of course, that poses no additional difficulties and can readily be handled by the same formulation even if with different boundary conditions.

3. Conclusions

We have introduced and verified a model for "*paralongitudinal*" approximations to the impedance of an elastic half-space. These allow to model shallow waves that are guided longitudinally within the ground above as well as along the superficial layers of half-space underneath. Within the half-space, the motions are assumed to decay exponentially with depth as well as laterally away from the embankment. That is, we assume implicitly that in the dispersion condition for the half-space

$$k_s^2 \equiv \left(\frac{\omega}{\beta}\right)^2 = k_x^2 + k_y^2 + k_z^2 \tag{15}$$

the longitudinal wavenumber in the half-space, say k_x, dominates over the other two ($k_x > k_s$), in which case the lateral wavenumbers k_y, k_z are purely imaginary and represent waves that decay exponentially with lateral and vertical distance to the embankment. This implies in turn that there is no radiation of energy into the half-space, or to the sides of the embankment. But this also means that the approximations provided, when used in the context of moving loads, cease to be applicable once these loads travel at supercritical ("transonic") speeds. But inasmuch as the vast number of engineering applications is for loads that travel at subcritical speeds, this is not an important shortcoming.

Author statement

Eduardo Kausel formulated the theory and João Barbosa worked on all demonstration examples shown in this article. Both worked on the text through an iterative process.

Declaration of competing interest

The authors declare that they have no known competing financial interests or personal relationships that could have appeared to influence the work reported in this paper.

Acknowledgments

The technical work described in this article received no external funding from any source. Thus, it represents curiosity-driven research.

Appendix 1. Paralongitudinal approximations to the half-space

The brief Matlab program shown in Fig. 7 can be used to obtain the paraxial approximations summarized in the ensuing:

$$z_{11} = \frac{4(1+a^2) - \xi^2(3a^4+1)}{2(1+a^2)^2}$$

$$z_{12} = \frac{4a^2(1+a^2) + \xi^2(1-a^2)^2}{2(1+a^2)^2}$$

$$z_{22} = \frac{4(1+a^2) - \xi^2(3+a^4)}{2(1+a^2)^2}$$

```
syms a x real
s = sqrt(1-x^2);
p = sqrt(1-a^2*x^2);
A = (1-s^2)/(1-p*s);
z11 = p*A;
z12 = -A+2;
z22 = s*A;
z11 = simplify(taylor(z11,5))
z12 = simplify(taylor(z12,5))
z22 = simplify(taylor(z22,5))

This produces the following results:

z11 = -1/2*(-4-4*a^2+3*x^2*a^4+x^2)/(1+a^2)^2
z12 = 1/2*(4*a^2+4*a^4+x^2+x^2*a^4-2*a^2*x^2)/(1+a^2)^2
z22 = -1/2*(-4-4*a^2+3*x^2+x^2*a^4)/(1+a^2)^2
```

Brief symbolic Matlab program to obtain the Taylor series expansion.

Appendix 2. The buffer layer

In the main body of this article we mentioned the need and convenience of adding a buffer layer with the same properties of the half-space when the latter is represented in terms of approximate impedances. Here we elaborate some further on why this is necessary. For this purpose, we consider the rather simple plane strain problem of a *single* discrete layer that is underlain by an elastic half-space while both are subjected to SH waves. As shown in Ref. [4], when the half-space is represented *exactly* below the discrete layer and the degree of freedom of the interface with the half-space is condensed out, one recovers at the surface of that combination the exact SH impedance. That this is so is nothing short of incredible, because the discrete layer cannot transmit waves of very high frequencies, yet the combination still works perfectly well for *any* frequencies and *any* horizontal wavenumbers.

Indeed, consider a single discrete layer of thickness h coupled to a half-space expressed in terms of its *exact* SH impedance. The combined impedance matrix is

$$\mathbf{K} = \begin{Bmatrix} K_{11} & K_{12} \\ K_{12} & K_{11} + K_{ex} \end{Bmatrix}$$

where the exact half-space impedance is

$$K_{ex} = \mu\, k\sqrt{1-\Omega^2}, \Omega = \frac{\omega}{k\beta} = \frac{V_{ph}}{\beta}$$

Also, using the so-called midpoint rule, the element impedances for the discrete (TLM) layer can be shown to be given by

$$K_{11} = \frac{\mu}{h}\left[\frac{1}{4}\kappa^2\left(1-\Omega^2\right)+1\right], K_{12} = \frac{\mu}{h}\left[\frac{1}{4}\kappa^2\left(1-\Omega^2\right)-1\right], \kappa = kh$$

The impedance of this combination as perceived from the upper surface follows then from the condensed impedance

$$K_{eq} = K_{11} - \frac{K_{12}^2}{K_{11}+K_{ex}} \equiv K_{ex} \vee k, \vee\omega$$

That this is so can readily be seen by assuming the identity to be true:

$$K_{11}(K_{11}+K_{ex}) - K_{12}^2 \equiv K_{ex}(K_{11}+K_{ex})$$

$$K_{ex}^2 = K_{11}^2 - K_{12}^2 \rightarrow K_{ex} = \sqrt{K_{11}^2 - K_{12}^2} = \mu k\sqrt{1-\Omega^2}$$

Astonishingly, we have recovered the *exact* SH impedance, and this no matter how thick the buffer layer should be. This is because the thickness ultimately drops out:

$$K_{11}^2 - K_{12}^2 = \left(\frac{\mu}{h}\right)^2 \left\{ \left[\frac{1}{4}\kappa^2(1-\Omega^2)+1\right]^2 - \left[\frac{1}{4}\kappa^2(1-\Omega^2)-1\right]^2 \right\}$$

$$= \left(\frac{\mu}{h}\right)^2 \left\{ \left[\frac{1}{4}\kappa^2(1-\Omega^2)+1+\frac{1}{4}\kappa^2(1-\Omega^2)-1\right] \left[\frac{1}{4}\kappa^2(1-\Omega^2)+1-\frac{1}{4}\kappa^2(1-\Omega^2)+1\right] \right\}$$

$$= \left(\frac{\mu}{h}\right)^2 \left\{ \left[\frac{1}{2}\kappa^2(1-\Omega^2)\right][2] \right\}$$

$$= \mu^2 k^2 (1-\Omega^2) \equiv K_{ex}^2$$

However, by the time that we replace the half-space by its approximation

$$K_{app} = \mu\, k\left(1 - \frac{1}{2}\Omega^2\right)$$

the condensed impedance will no longer be exact:

$$K_{eq} = K_{11} - \frac{K_{12}^2}{K_{11} + K_{app}} \neq K_{ex}$$

Still, the ratio $R = K_{eq}/K_{ex}$ is close to 1 for a broad set of wavenumbers $k > \omega/\beta$ (such that $V_{ph} < \beta$). For example, Fig. 8 shows this ratio when $h = 1$, $k > 1$, $\Omega = 0.8$. As can be seen, $R \approx 1$ in the entire range of wavenumbers. Moreover, for phase velocities satisfying the restriction $\Omega < 0.8$, the ratio equals 1 for practical purposes.

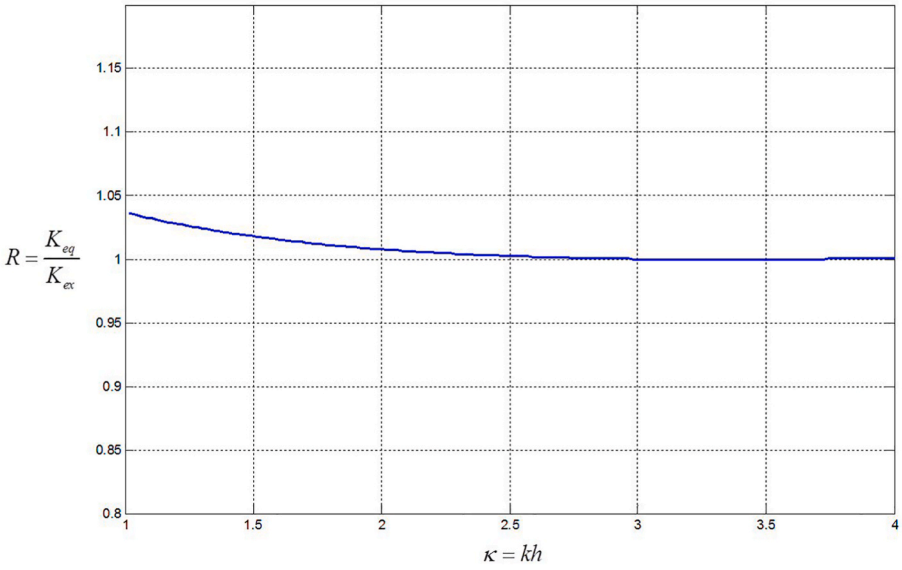

Fig. 8. Ratio of apparent stiffness to exact stiffness for $\Omega = V_{ph}/\beta = 0.8$.

By way of contrast, the ratio K_{app}/K_{ex} is not anywhere near as good (i.e. close to 1). Hence, we conclude that adding a buffer layer is a necessity for the accurate representation of the half-space. Similar (even if more complicated expressions) apply also the SVP case.

In general, it behooves to choose a buffer whose thickness is roughly equal to four times the depth of the soil times the ratio of shear wave velocity in the half-space and the average of the shear wave velocity in the soil. In the example shown in the text, this is $h_{buffer} \sim (4)(0.6)(300)/(200) = 3.6$ m. This is the wavelength in the half-space that corresponds to a quarter-wavelength in the soil. The buffer layer should be so constrained that it reproduces the behavior of the plane-strain modes (constrain the lateral motions for the symmetric modes, and the vertical-longitudinal motion for the antisymmetric modes).

References

[1] Kausel E, Peek R. Dynamic loads in the interior of a layered stratum: an explicit solution. Bull Seismol Soc Am 1982;72(5):1459–81.

[2] Kausel E. Wave propagation in anisotropic layered media. Int J Numer Methods Eng 1986;23:1567–78.

[3] Barbosa JM de O, Park J, Kausel E. Perfectly matched layers in the thin layer method. Comput Methods Appl Mech Eng 2012;217–220:262–74.

[4] Kausel E. Can a discrete dynamic model ever perfectly simulate a continuum? Soil Dynam Earthq Eng 2018;112:53–7.

[5] Barbosa JM de O. Analysis and mitigation of vibrations induced by the passage of high-speed trains in nearby buildings. PhD thesis. Portugal: Faculty of Engineering at the University of Porto; 2013.

[6] Alves Costa P, Calçada R, Silva Cardoso A. Track-ground vibrations induced by railway traffic: in-situ measurements and validation of a 2.5D FEM-BEM model. Soil Dynam Earthq Eng 2012;32:11–128.

[7] Jin Q, Thompson DJ, Lurcock EJ, Toward MGR, Ntotsios E. A 2.5 D finite element and boundary element model for the ground vibration from trains in tunnels and validation using measurement data. J Sound Vib 2018;422:373–89.

[8] Kuo KA, Verbraken H, Degrande G, Lombaert G. Hybrid predictions of railway induced ground vibrations using a combination of experimental measurements and numerical modeling. J Sound Vib 2016;373:263–84.

[9] Lombaert G, Degrande G. Ground-borne vibration due to static and dynamic axle loads of InterCity and high-speed trains. J Sound Vib 2009;319:1036–106611.

[10] Rodríguez-Rozas A, Pardo D, Torres-Verdín C. Fast 2.5D finite element simulations of borehole resistivity measurements. Comput Geosci 2018;22:1271–81.

[11] Sheng X, Jones CJC, Thompson DJ. Modeling ground vibration from railways using wavenumber finite- and boundary element methods. Proc. Roy. Soc. A 2005;461:2043–70.

[12] Tadeu A, António J, Simões N. 2.5D Green's functions for transient heat conduction problems in layered formations. In: Transactions on modelling and simulation, vol. 35. Southampton, UK: WIT Press; 2003.

[13] Zhao J, Huang X, Liu W, Zhao W, Song J, Xiong B, Wang S. 2.5-D frequency-domain viscoelastic wave modeling using finite-element method. Geophys J Int 2017;211:164–87.
[14] Kausel E, Roësset J. Stiffness matrices for layered soil. Bull Seismol Soc Am 1981; 71:1743–61.
[15] Kausel E. Fundamental solutions in elastodynamics: a compendium. Cambridge, England: Cambridge University Press; 2006.
[16] Kausel E, Roësset JM. Frequency domain analysis of undamped systems. J Eng Mech 1992;118(4):721–34.
[17] Kumar J, Naskar T. A fast and accurate method to compute dispersion spectra for layered media using a modified Kausel-Roësset stiffness matrix approach. Soil Dynam Earthq Eng 2017;92:176–82.
[18] Kausel E, Estaire J, Crespo-Chacón I. Proof of critical speed of high-speed rail underlain by stratified media. Proc. Roy. Soc. A 2020;476(2240):1364–5021.
[19] Kausel E, Malischewski P, Barbosa J de O. Osculation of spectral lines in a layered medium. Wave Motion 2016;56:22–42.